Partitioning and Availability of Metals from Water Suspended Sediments: Potential Pollution Risk Assessment

Magaly Cabral-Lares [1], Marusia Rentería-Villalobos [1,*], Aurora Mendieta-Mendoza [1], Ziury Ortíz-Caballero [1], Elena Montero-Cabrera [2] and Ignacio Vioque [3]

1   Departamento de Recursos Naturales, Facultad de Zootecnia y Ecología, Universidad Autónoma de Chihuahua, Perif. Ramiro Almada km 1, Chihuahua 31453, Mexico; rocio.cabral@cimav.edu.mx (M.C.-L.); auroramendieta2516@gmail.com (A.M.-M.); ziury.ortiz@cimav.edu.mx (Z.O.-C.)
2   Centro de Investigación en Materiales Avanzados, CIMAV, Miguel de Cervantes 120, Chihuahua 31109, Mexico; elena.montero@cimav.edu.mx
3   Departamento de Física Aplicada II, Facultad de Arquitectura, Universidad de Sevilla, Av. Reina Mercedes, 41004 Sevilla, Spain; ivioque@us.es
*   Correspondence: mrenteria@uach.mx; Tel.: +52-614-4340304

Abstract: The water management initiatives in freshwater systems focus on water availability to preserve this resource for human uses and the health of aquatic ecosystems. This work presents an assessment of the potential pollution risk caused by the metal availability in suspended sediments. The objective of this study was to determine the partitioning, association, and geochemical fractionation of metals in suspended sediments from a surface water body. Additionally, the environmental assessment for this reservoir was estimated using geoaccumulation, enrichment, and pollution indices of metals and the related potential risk by their elemental availability (RAC). Chemical, mineralogical, and morphological characterizations were obtained by inductively coupled plasma spectrometry, alpha spectroscopy, X-ray crystallography, and scanning electron microscopy. Clay, quartz, montmorillonite, and calcite were the main minerals of suspended sediments. Chemical fractionation was the parameter affecting the concentrations of metals in suspended sediments. The sediment composition is of natural origin; however, these finer particles can promote the scavenging of toxic metals. It contributes to obtaining moderate to high levels for enrichment/contamination indices. Although Ca, Mg, and U were the most accessible metals for aquatic biota, metals such as Sr, Mn, Li, Cu, and Ni in the exchangeable phase of suspended sediments are the potentially toxic elements in this aquatic ecosystem.

Keywords: chemical fractions; suspended particulate matter; metal release; metal co-occurrence; aquatic environment; surface water

1. Introduction

There is an urgent need to balance social, economic, and environmental sustainability globally. Water scarcity is a severe problem due to dwindling surface and groundwater supplies caused by natural and human sources; these water changes adversely affect its availability [1]. In nature, water availability depends on climatic and geological factors [2], where their interaction has been called hydrogeologic environment [3].

Water quality conditions are essential for functioning in the ecosystem and meeting human commitments. Those systems naturally contain trace elements responsible for a fraction of the biota's dose from the environment [4,5]. The indices such as enrichment factor, Geoaccumulation Index, contamination factor, and potential ecological risk index are used to determine the pollution risk given by metals [6–11]. However, most of those studies have been widely evaluated using the bottom sediments. Nevertheless, low-weight sediments remain in suspension, which can be mobilized through long distances, being a valuable transport source of pollutants [12–14].

The concentration of toxic elements is generated through lixiviation, chemical speciation, size of suspended sediments, and movement, resulting in their transport and distribution within a water body [15]. In this regard, processes such as diffusion and dispersion, transport, exchange in solid-solution phases, and sorption/desorption control the migration of the contaminants in water bodies [7,16–18]. Furthermore, environmental conditions influence the sorption of contaminants on suspended sediments, which can change to soluble states and be available to other organisms [19,20]. Chemically, element fractionation is controlled by chemical properties such as oxidative state, chemical affinity, chemical species competition, among others. Therefore, evaluating the availability of elements in suspended sediments should be a priority to establish the potential toxicity. The particle fractions can be [21–24]: bioavailable (exchangeable/soluble metals in water), reduced (metals linked to oxides freed when conditions change from oxic to anoxic), oxidized (metals linked to organic components and sulfides, freed under oxidant conditions), and residual (elements strongly connected to the crystalline minerals structures). Due to the chemical species, contents in gross sediments can be a poor indicator of metal releasing in aquatic ecosystems; it is critical to identify the bioavailability of metals in suspended sediments under variations of environmental conditions. The objective of the present study was to determine the partitioning, association, and geochemical fractionation of metals (including ^{238,234}U and ^{232,230}Th) in suspended sediments from surface water to assess the potential pollution risk for an aquatic environment.

2. Materials and Methods

2.1. Study Site

The present study was performed in the San Marcos reservoir, located between 28°55′ and 28°40′ latitude N and between 106°10′ and 106°25′ longitude W, in the municipality of Chihuahua. This reservoir is one of the oldest reservoirs in Chihuahua, Mexico, built-in 1905, before the Mexican revolution. This region is placed in a volcanic caldera, showing rhyolitic tuffs and some Upper Cenozoic volcanic rocks with intermediate to basic composition [25,26]. Likewise, basalts and a few calcareous rock outcrops can be found [25]. Due to its high topographic elevations, the San Marcos region serves as a source of water recharge for the Chihuahua–Sacramento aquifer. In this semiarid zone, short periods of rain are present with annual precipitation from 200 to 600 mm, where temperatures can reach up to 38 °C [27].

The San Marcos reservoir is fed with water from two rivers (Blanco and San Marcos rivers) and a spring, where San Marcos River is the primary source of recharge to this reservoir. This river comes in contact with two uranium deposits (Victorino and San Marcos outcrops) present in the area, contributing natural radioisotopes to this reservoir [28]. Several decades ago, some mining studies were carried out in these mineral deposits to benefit uranium extraction; however, it was concluded that there was no feasibility for uranium mining. The spring is located on the north-eastern slope of the reservoir and provides abnormal uranium and radon concentrations due to its groundwater origin [28,29]. This zone uses the surface and ground waters for agricultural and domestic activities and human consumption. The location of the study area is shown in Figure 1.
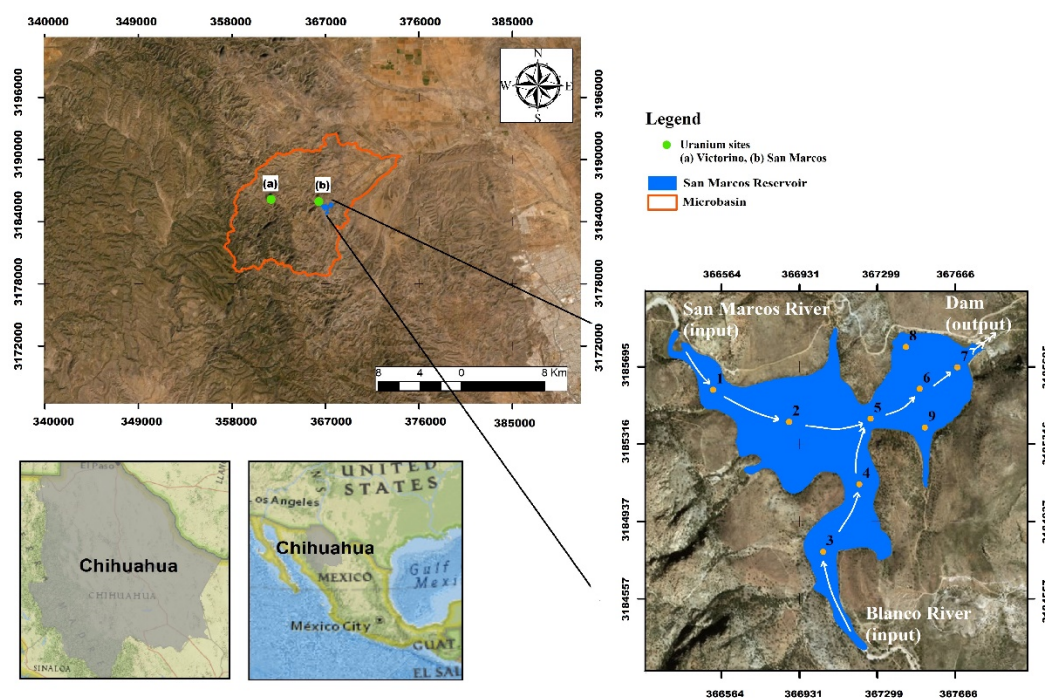
Figure 1. Satellite image of the study area. Distribution of the sampling points, from 1 to 9 along the flux water, in the San Marcos reservoir.

2.2. Sampling

Eighteen sampling sites were collected along the flux water of San Marcos reservoir in May 2016, before the rainy season; nine of those were taken at the surface level (40 cm below from the topwater) and the other nine at a deep level (1 m above from the reservoir bottom). Input water corresponds to sampling points 1 (San Marcos River), 3 (Blanco River), and 8 (spring). Every water sample was collected in plastic containers of 50 L; before sampling, these containers were acid washed in the lab and in situ pre-equilibrated with water from every sampling. According to Mexican regulation, 1 L of water was also collected to determine water quality parameters in every sampling point [30].

2.3. Sample Analysis

2.3.1. Water and Sediments Samples

Parameters such as pH, temperature (T), oxidation-reduction potential (ORP), and total dissolved solids (TDS) were recorded in situ. While pH, T, and TDS were obtained using multiparametric equipment (Hanna, Hl98130), the ORP was measured with an ORP tester (OAKTON, Waterproof ORPTestr Double junction). Total alkalinity, chlorides, and total hardness were determined by the methodology proposed in the Mexican regulations [31–33]. The analysis of sulfates and nitrates were performed through Hach procedures by 8039 (Cadmium reduction method) and 8051 (SulfaVer 4) methods and measured using a Hach spectrophotometer (Hach, DR 2010) [34], whereas Ca, Mg, Na, and K were determined using an atomic absorption spectrophotometer (GBC Avanta Sigma, Melbourne, Australia), following the methodology suggested in the regulation [35].

The 50 L water samples were exposed to successive filtrations to obtain the suspended sediments and dissolved phase. Although suspended sediments are composed of particles of different diameters, in this work, two sizes of particles were analyzed: coarse (>25 μm) and fine (25 μm > particles > 11 μm). Initially, water samples were passed through a cellulose filter with a pore size of 25 μm (coarse particles); subsequently, that water was filtered with a pore size filter of 11 μm to obtain the fine particles. For purposes of this work, the liquid phase obtained from the final filtration was also analyzed and called the dissolved phase.

2.3.2. Characterization of Suspended Sediments and Dissolved Phase

Scanning Electron Microscopy

The coarse and fine particles were characterized using SEM in a JEOL 6460LV, obtaining secondary electron images (SEI) and back-scattered electron images (BEI); with a maximum resolution of 3.5 nm. This device was coupled to a microprobe EDX and equipped with a Beryllium window ATW2 (resolution 137 EVAT 5.9 KeV) for semi-quantitative analysis using the Oxford INCA® software.

X-ray Diffraction

The suspended sediments were subjected to a mineral analysis through X-ray diffraction, using an XPERT-PRO PANalytical® (Radiation of Cu pipes with Kα radiation, 40 mA and 40 kV). The diffraction patterns were obtained at an angular interval of 2θ from 4 to 70°, with steps of 0.05° and 2 s exploration time. The pattern analysis was performed using the Data Collector® software.

Chemical Analysis

The coarse and fine particles underwent a chemical procedure to obtain the bioavailable, reduced, oxidized, and residual fractions. The sequential extraction procedure to obtain each fraction is described by [22,23,36,37]. Subsequently, the concentration of major and trace elements in coarse and fine particles (bulk particles), particle fractions, and dissolved phase was determined by ICP-OES, whereas U and Th isotopes were obtained using alpha spectrometry.

Element Characterization

Aliquots of bulk particles, particle fractions, and dissolved phase were digested using a microwave (ON 60 Hz Anton Paar, Graz, Austria). The element concentrations were obtained using an ICP-OES Optima 8300® (Perkin Elmer®, USA; software version 1.10); a calibration standard of 21 elements (Perkin Elmer, Waltham, MA, USA, LLC STD-AS QC 21 Elements) to calibrate this equipment. For the quality/accuracy control, sediment samples were analyzed by triplicate, and a certified reference material (IAEA-375) was measured; it was treated under the same sequential extraction procedure, fractionation of elements. The element recovery (%) was obtained by comparing the concentration of each element in bulk samples and the sum of concentrations in four fractions. The measurement precision was below 30% of RSD (relative standard deviations), while average recovery rates of element concentrations were between 80 and 110%. In this study, the elements reported were those in which most concentrations were above their respective detection limit.

Radiological Characterization

Radiological characterization was carried out only in suspended sediments at the bottom level. Thus, the contents of U and Th isotopes were determined in bulk particles, particle fractions, and dissolved phase. Internal standards of ^{232}U (117 $\pm$ 0.6 mBq/g) and ^{229}Th (104.04 $\pm$ 0.6 mBq/g) were added, through which the activities of the isotopes of interest were obtained. Each aliquot underwent a process of digestion, extraction, separation, and purification (deposition) of radioisotopes. The radioisotopes U and Th were obtained through alpha spectrometry with surface barrier detectors (Canberra ®Alpha, Atlanta, GA, USA), and the analysis of alpha spectrums was performed with the Genie 2000® software. The spike recoveries ranged from 84 to 96% and from 55 to 78% for U and Th, respectively.

2.4. Distribution Coefficient (kd)

The distribution of elements between suspended sediments and dissolved phase was obtained by the distribution coefficient, kd [38,39], Equation (1):

$$kd = \frac{Cis\left(\frac{mg}{kg}\right)}{Ciw\left(\frac{mg}{L}\right)},$$

(1)

The kd is the element concentration ratio, Cis is the concentration of the i-element in the suspended sediments, and Ciw is the concentration of the i-element in the dissolved phase.

2.5. Statistical Analysis

Compositional data analysis (CoDA) methods are necessary due to the compositional nature of geochemical data [40]. Therefore, a Shapiro–Wilk test was employed to analyze the normal distribution of these data. As non-normal distribution was observed, results were log-transformed using the R software (www.rproject.org (accessed on 1 January 2022)) and analyzed by: (a) an ANOVA, to identify the interaction effects of sampling point and water depth in the physicochemical parameters, applying the procedure GLM using the package SAS® [41]; (b) an ANOVA, to identify the interaction effects of sampling point, particle size, fractionation of elements, and water depth in the elemental composition of suspended sediments, applying the procedure GLM using the package SAS®; (c) a distribution of elements using cluster heatmaps (isometric log-ratio transformation) using the R-package robCompositions (pivotCoord and gplots functions); (d) a correlation analysis between the implicit continuous variables, using the R-procedures ggplot2 and corrplot; and (e) a multivariate analysis, Factorial Analysis (FA), using the isometric log-ratio (ilr) transformation methods through the R-function "factanal" [42–44].

2.6. Potential Pollution Risk Assessment

Element concentrations from suspended sediments were used to identify their enrichment, pollution levels, and the potential pollution risk [6,7,45,46]. Due to element recoveries being greater than 80%, the analysis of indices was carried out using the sum of element concentrations obtained by fractions (F1–F4). Furthermore, to provide an improved prediction of the potential risk for aquatic biota, the element concentrations from the available sediment fractions (bioavailable, F1; reduced, F2; and oxidized, F3) were used to calculate the Risk Assessment Code (RAC).

2.6.1. Contamination Factor (Cf)

The Cf is a single index used to monitor the element status in sediment [7,11,16]. This index was obtained by Equation (2):

$$Cf = Ci/Ci_{earth\ crust}$$

(2)

where Ci is the i-element concentration in sediment and $Ci_{earth\ crust}$ is the i-element concentration in the upper continental crust. According to [11], Cf is classified as Cf < 1 low contamination factor, $1 \leq Cf < 3$ moderate contamination factor, $3 \leq Cf < 6$ considerable contamination factor, and Cf > 6 very high contamination factor.

2.6.2. Enrichment Factor (Ef)

The Ef was obtained by the normalized ratio from sediment element concentrations to those in the average upper continental crust [47,48]. This normalization takes into consideration variations in sediment grain size and mineralogy. The Ef was calculated by Equation (3):

$$Ef = (Ci/Re)_{sediments}/(Ci/Re)_{earth\ crust}$$

(3)

Ci is the i-element concentration in sediment, and Re is the reference element. The reference element must be stable and associated with finer particles; elements such as

Al, Fe, Mn, Rb, and Ti are widely used [16,45]. In this work, Fe was used as Re due to is one of the major constituents in clay material [11,49–51]. Ef is classified as Ef < 1 deficient/not enriched, 1 < Ef < 3 minor enrichment, 3 < Ef < 5 moderate enrichment, 5 < Ef < 10 moderate-severe enrichment, 10 < Ef < 25 severe enrichment, 25 < Ef < 50 very severe enrichment, and 50 < Ef extremely severe enrichment.

2.6.3. Geoaccumulation Index (Igeo)

The Igeo defines the metal concentration in fine fraction particles and detects the anthropogenic influence [45]. This index is expressed by Equation (4):

$$\text{Igeo} = \log_2 (C_i/1.5 \times Bn) \tag{4}$$

where C_i is the i-element concentration in sediment, Bn is the geochemical background concentration of the element, and 1.5 is the constant to analyze natural fluctuations in the element contents. Its classification is uncontaminated Igeo < 0, uncontaminated-moderately contaminated 0 < Igeo < 1, moderately contaminated 1 < Igeo < 2, moderately heavily contaminated 2 < Igeo < 3, heavily contaminated 3 < Igeo < 4, heavily extremely contaminated 4 < Igeo < 5, and extremely contaminated 5 < Igeo.

2.6.4. Metal Availability Assessment

Metals in available fractions of sediments are the main responsible for pollution risk. The secondary to primary metal phases ratio (SPR) and the Risk Assessment Code (RAC) were evaluated to obtain the potential pollution risk by releasing metals from suspended sediments.

The SPR was calculated by the ratio of metal concentrations in secondary fractions (F1, F2, and F3) to those in primary fraction (F4) [52]. The SPR and RAC were obtained using the Equations (5) and (6), respectively:

$$\text{SPR} = C_{F1\text{-}3}/C_{F4} \tag{5}$$

where $C_{F1\text{-}3i}$ is the sum of i-element in F1 (bioavailable), F2 (reduced), and F3 (oxidized); and C_{F4i} is the concentration of the i-element in residual fraction (F4).

$$\text{RAC } (\%) = C_{F1\text{-}2}/C_{Ti} \tag{6}$$

where $C_{F1\text{-}2}$ is the sum of i-element concentrations in the most labile fractions (F1 and F2), and C_{Ti} is the total concentration of i-element obtained by the sum of their concentrations from all fractions. RAC is classified as no risk < 1, low risk 1–10, medium risk 11–30, high risk 31–50, and very high risk > 50 [6,36].

3. Results

3.1. Bulk Water Quality

The physicochemical parameters and chemical species obtained in bulk samples from the San Marcos reservoir are summarized in Table S1 (Supplementary Material). The pH was neutral at the surface and deep levels of this water body, as well as the ORP showed mainly sub-oxic conditions. In addition, alkalinity at surface level ranged from 14 to 17 mg $CaCO_3$/L, whereas at high depth, 34 to 36 mg $CaCO_3$/L was found. Likewise, the dissolved ions were found in the following abundance $SO_4^{2-} > Na^+ > Cl^- > K^+ > NO_2^- > Ca^{2+} > Mg^{2+}$.

3.2. Mineral Composition of the Suspended Particulate Matter

The mineral analysis of the fine and coarse particles showed that, in general, the main minerals contain Ca, Si, feldspars, and clays. The main mineral species found were Calcite [$Ca(CO_3)$], Quartz [(SiO_2)], Albite [($Al_{1.2}Ca_{0.2}Na_{0.8}O_8Si_{2.8}$)], and Montmorillonite [$Ca (Al_2Si_4O_{11} (OH))$].

3.3. Morphology and Elemental Composition

The results of the particle morphology are shown in Figure 2. The coarse and fine particles are amorphous with a rough and porous surface. Coarse particles show dimensions in a range from 30 to 150 μm. These particles showed differences on their surface: accumulation of small particles (Figure 2a), lightly smooth angles (Figure 2b), and sharp edges (Figure 2c). In addition, fine particles are composed of particle aggregates with dimensions from 13 to 227 μm (Figure 2d–f); it indicates a high surface charge for this particle size, attracting each other to form fine particle agglomerates. Furthermore, coarse particles are mainly composed of Si (35%), Na (23%), and Fe (14%), whereas fine particles are composed of Si and Ca with 41% and 20%, respectively.

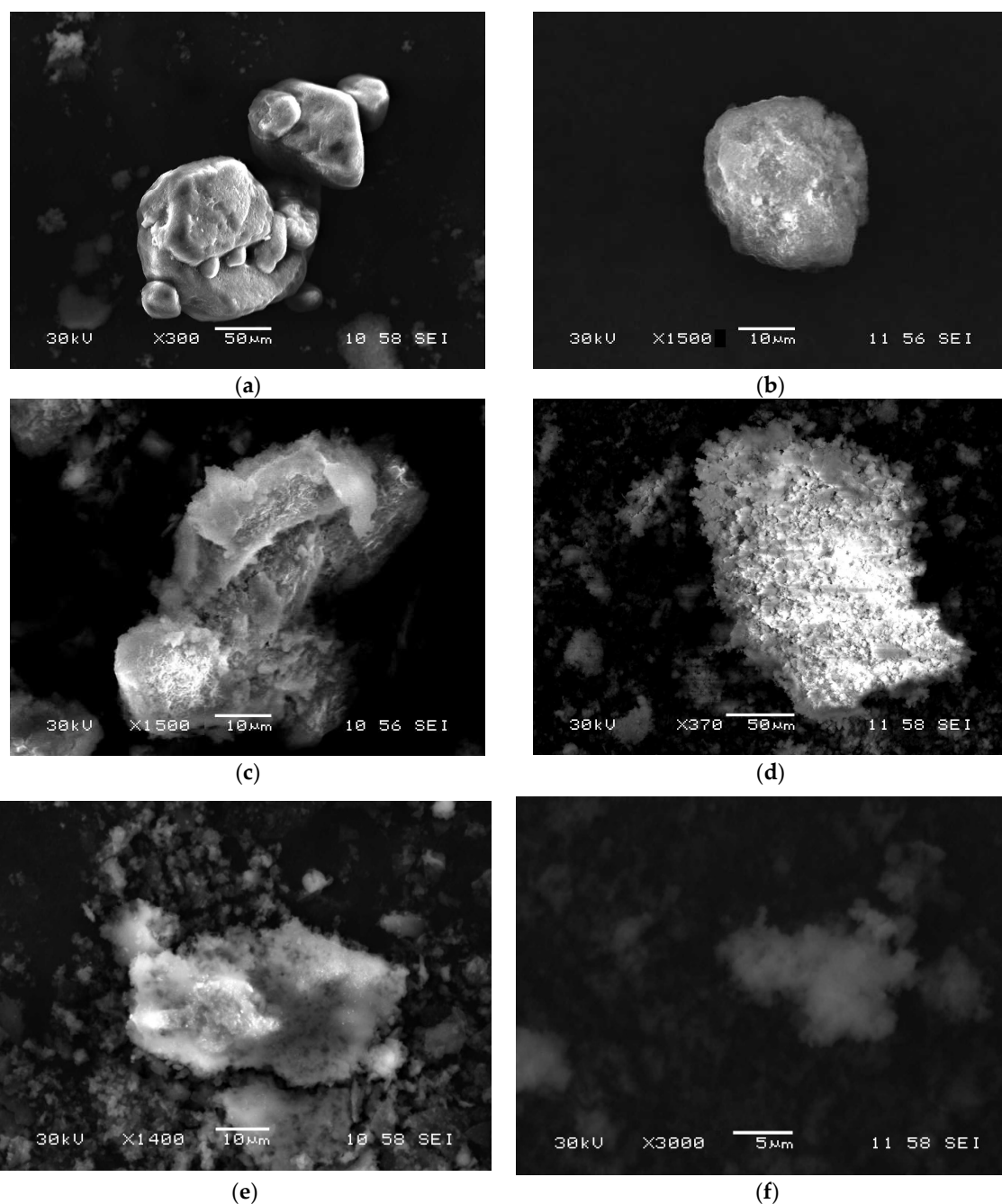(**a**)

(**b**)

(**c**)

(**d**)

(**e**)

(**f**)

Figure 2. Morphological analysis with secondary electrons of the suspended particulate matter. Coarse particle dimensions: (**a**) 130 × 150 μm, (**b**) 30 × 35 μm, and (**c**) 50 × 60 μm. Fine particles dimensions: (**d**) 160 × 227 μm, (**e**) 51 × 84 μm, and (**f**) 13 × 17 μm.

3.4. Partitioning of Chemical Species

The concentrations of major and trace elements in suspended particles and dissolved phase are summarized in Table S2 (Supplementary material) at the surface and deep level.

3.4.1. Physicochemical Parameters

From one factor analysis, the concentrations of elements were significantly different according to depth ($p < 0.05$), but they were not for the sampling point. The alkalinity ($CO_3^=$, HCO_3^-), sulfates (SO_4^{2-}), calcium (Ca^{2+}), and sodium (Na^+) showed higher concentrations at the deeper water level, except for Na^+. Likewise, the interaction effects depth-sampling point did not show significant differences.

Moreover, some distribution differences of physicochemical parameters related to levels were identified with the heatmaps of correlation coefficients. Figure 3 shows log-transformed parameters sorted according to cluster analysis [53]. The distribution of physicochemical parameters to both levels indicated two main subgroups by clustering ($p < 0.05$). At the surface level, the NO_2, Mg^{2+}, Ca^{2+}, K^+, Na^+, and ORP form the first subgroup; this can be seen at the lower-left corner of Figure 3a. The highest positive correlations of those parameters were $NO_2 - Mg^{2+}$ and $Ca^{2+} - K^+$ (R > 0.70), whereas $Na^+ - ORP$ showed a weak correlation (R = 0.5). The second subgroup comprises TDS, Alkalinity, pH, SO_4^{2-}, Cl^-, T, and hardness (Figure 3a, upper right corner). In the deep level, the subgroup to the upper right corner in Figure 3b showed a high number of parameters that were positively correlated (pH, Alkalinity, Hardness, TDS, T, SO_4^{2-}, ORP, Mg^{2+}, Na^+, and Cl^-), whereas NO_2 and K^+ remain clustered as another subgroup (R > 0.62).

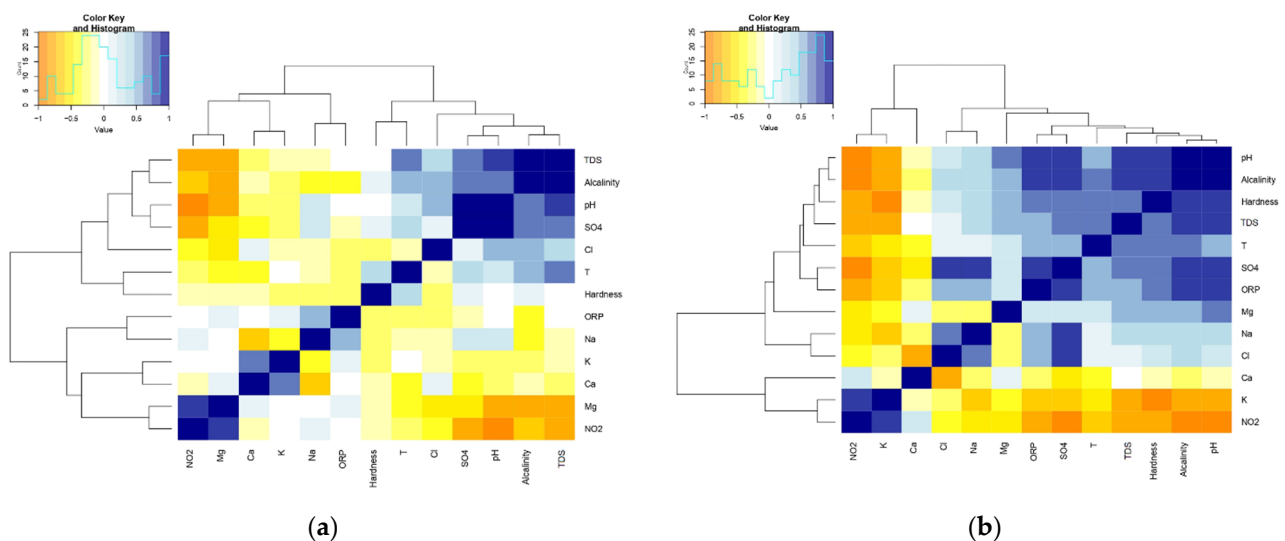(a)   (b)

Figure 3. Heatmaps of physicochemical parameters for: (**a**) surface level and (**b**) deep level. The strength of color indicates the strength of correlation. Blue colors indicate positive correlations, light colors (yellow/orange) indicate negative correlations.

3.4.2. Particle Composition

In Table 1 are shown the results of principal components and the kd. Most of the elements are concentrated in suspended sediments showing kd >> 1 Lkg^{-1}. These metals showed kd in the following sequence Ti > Mn > Fe ≈ Ni ≈ V ≈ Cu ≈ Li ≈ Pb ≈ Zn > Mg ≈ Ca ≈ Sr. Statistically, major and trace elements explain >91% of the variance in PC1, showing a high correlation (R > 0.9, $p < 0.05$) for both particle sizes and at both depth levels. It confirms the natural origin of these elements in suspended sediments.

Table 1. Principal component analysis and distribution coefficient (kd; L/kg) of the suspended sediment samples.

Variable	Components				kd	
	Coarse Particles		Fine Particles		Coarse Particles	Fine Particles
	PC1	PC2	PC1	PC2		
Surface level						
Fe	0.284	−0.006	0.302	0.05	9.0×10^2	7.4×10^2
Mg	0.284	−0.034	0.301	−0.002	1.3×10^1	2.0×10^1
Ca	0.284	−0.016	0.302	0.038	9.9×10^0	2.6×10^1
Mn	0.284	0.011	0.296	0.098	1.1×10^4	5.1×10^3
Pb	0.279	0.253	0.302	−0.052	5.2×10^1	1.7×10^2
V	0.275	0.072	0.278	−0.109	1.7×10^2	2.4×10^2
Ni	0.207	−0.937	−0.042	0.73	2.5×10^2	2.3×10^2
Ti	0.283	0.097	0.302	0.045	-	-
Sr	0.284	−0.022	0.301	0.09	1.0×10^1	3.3×10^1
Cu	0.284	0.062	0.302	0.059	7.1×10^1	3.0×10^2
Li	0.281	0.182	0.302	0.045	6.8×10^1	3.1×10^2
Zn	0.284	0.029	0.301	0.088	4.3×10^1	1.5×10^2
U *	-	-	-	-	-	-
Autocorrelation	12.36	0.53	10.89	1.73		
Variance (%)	95.1	4.1	83.8	13.3		
Accumulated variance (%)	95.1	99.2	83.8	97.1		
Deep level						
Fe	0.289	0.086	0.281	0.141	2.6×10^2	3.9×10^3
Mg	0.289	0.076	0.281	−0.145	6.8×10^0	9.4×10^1
Ca	0.287	0.145	0.281	0	5.7×10^0	3.7×10^1
Mn	0.288	0.122	0.279	0.248	7.7×10^3	1.0×10^5
Pb	0.279	−0.163	0.276	−0.268	1.4×10^1	1.3×10^2
V	0.135	−0.924	0.266	−0.655	5.1×10^1	8.2×10^2
Ni	0.283	−0.017	0.27	0.049	1.5×10^2	5.5×10^2
Ti	0.287	0.114	0.272	0.512		
Sr	0.289	0.053	0.281	−0.128	2.9×10^0	2.0×10^1
Cu	0.289	0.053	0.279	0.225	3.5×10^1	1.3×10^2
Li	0.288	0.053	0.281	0.079	2.5×10^1	1.2×10^2
Zn	0.288	0.096	0.281	0.13	3.2×10^1	1.3×10^2
U *					8.7×10^0	2.3×10^1
Autocorrelation	11.89	0.91	12.61	0.25		
Variance (%)	91.5	7	97	1.9		
Accumulated variance (%)	91.5	98.5	97	98.9		

* It was calculated as total uranium, sum of ^{238}U and ^{234}U concentrations.

From ANOVA analysis, the element concentrations did not show significant differences ($p < 0.05$) according to depth and particle size, see Figure S1 in supplementary material; however, their concentrations were different by particle fractions. Heatmap, based on symmetric coordinates for element concentration by particle fractions, are presented in Figure 4. Uranium and thorium were not included in these analyzes.

The fractionation and co-occurrence of major elements indicate that Ca and Mg tend to be in the bioavailable fraction (F1), Fe and Mn in the reduced fraction (F3), and Ti in the residual fraction (F4), see Figure S1, supplementary material. Besides, trace elements such as Sr, Li, and Zn were mainly concentrated in F1, while the highest contents of Pb were in F2. Finally, Cu, Ni, and V tended to be in the residual fraction.
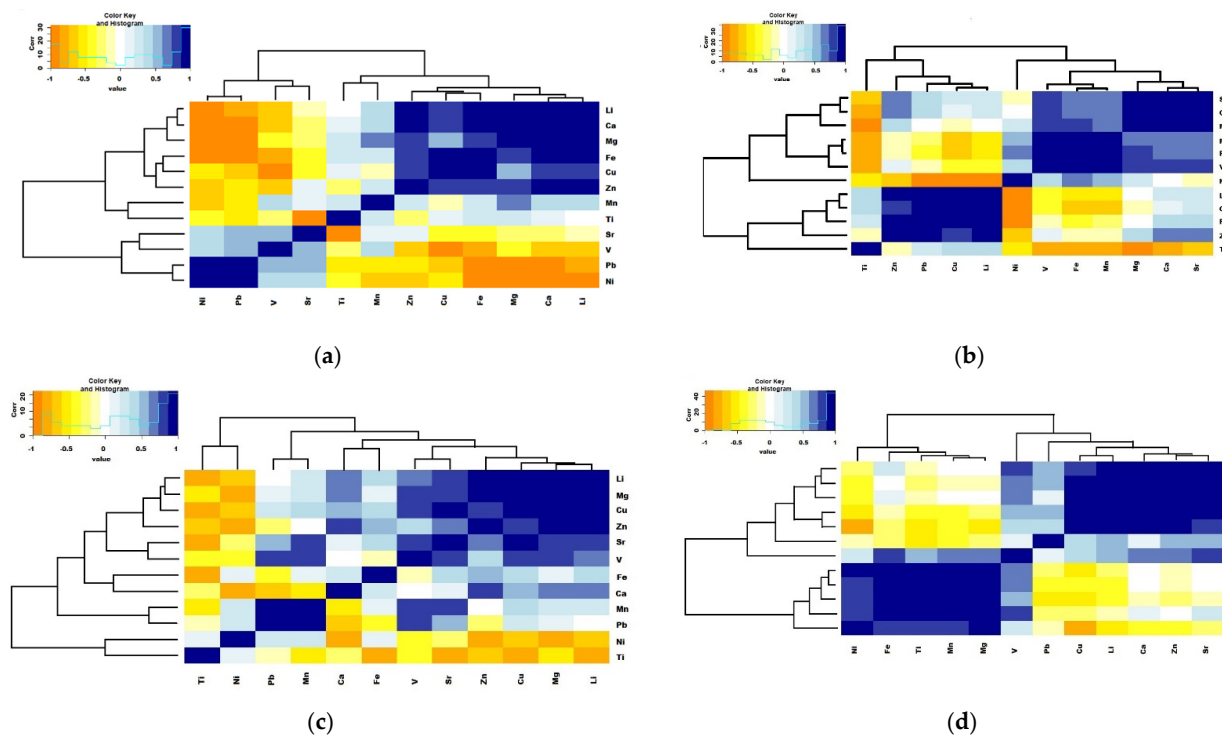
(a)

(b)

(c)

(d)

Figure 4. Fractionation of metal: (**a**) bioavailable fraction (F1); (**b**) reduced fraction (F2); (**c**) oxidized fraction (F3); and (**d**) residual fraction (F4).

3.5. Isotopic Determination

U radioisotopes showed higher concentrations in fine particles than in coarse particles. In contrast, Th radioisotope concentrations were similar in both particle sizes ($p < 0.05$). The concentrations of ^{238,234}U and ^{232,230}Th are shown in Table 2. Likewise, Figure S3 in supplementary material shows the ^{238,234}U and ^{232,230}Th contents by chemical fractions. While the highest mean concentrations of ^{238}U and ^{234}U were found in the bioavailable fraction of fine particles, high concentrations of ^{230}Th and ^{232}Th were found in residual fractions of both particles.

Table 2. Partitioning of ^{238,234}U and ^{232,230}Th, mBq kg^{-1}, and their activity ratios, in fractions of suspended sediments at high depth.

	Coarse	Coarse$_{sum}$ *	Fine	Fine$_{sum}$ *	Dissolved [1]
^{238}U	45 26–57	65 16–90	125 90–152	197 78–482	5.3 2–9.7
^{234}U	87 44–159	111 30–171	142 100–189	320 175–471	30 10–70
^{232}Th	nm [a]	74 18–104	49 31–74	79 43–133	nm
^{230}Th	nm	64 7–92	169 101–246	78 43–160	nm
^{234}U/^{238}U	2.1 1.2–3.0	1.7 1.5–1.9	1.2 0.8–1.5	2.1 1–3.5	6.3 1.5–10.5
^{230}Th/^{232}Th	-	0.8 0.4–1.0	3.6 2.3–5.0	1.0 0.8–1.2	-
^{232}Th/^{238}U	-	1.1 1.0–1.3	0.4 0.2–0.8	0.6 0.1–1.0	-
^{230}Th/^{238}U	-	0.9 0.4–1.2	1.5 0.7–2.7	0.6 0.1–1.0	-

* The total concentration was obtained from the average concentration in every fraction and averaging the mean from each sampling point. [1] The concentration of elements is given in mBq L^{-1}. [a] No measured.

3.6. Potential Pollution Risk

Figure 5 shows the results of the indices that evaluate the status of metals in suspended sediments. Elements such as Cu, Li, Mn, Pb, and Zn showed contamination indices values (Ef, Igeo, and Cf) << 1, mainly in fine particles. These metals reached a very high level of Cf, severe enrichment, and tended to show moderately heavily contaminated levels by Igeo values. Conversely, Ni, Sr, and V showed lower values for these indices.
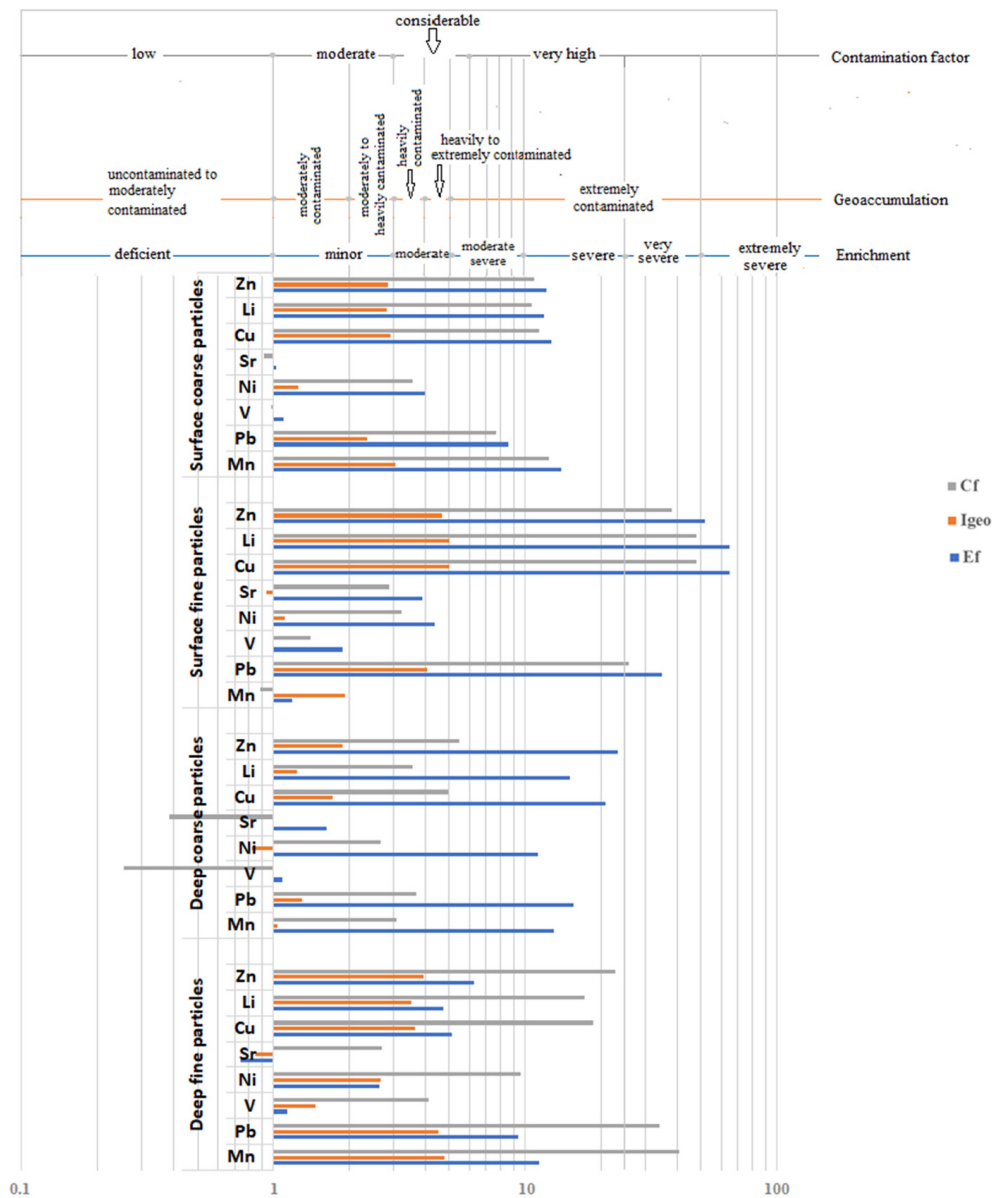

Figure 5. Results of Cf, Igeo, and Ef produced by metals in suspended sediments.

On the other hand, the SPR ranged from 0.4 to 238 values, where Ca, Mn, and Pb showed the highest SPR-values, see Figure 6. Likewise, the highest RAC percent (>20%) were shown by Mg, Ca, Mn, Cu, Li, Sr, and Zn.
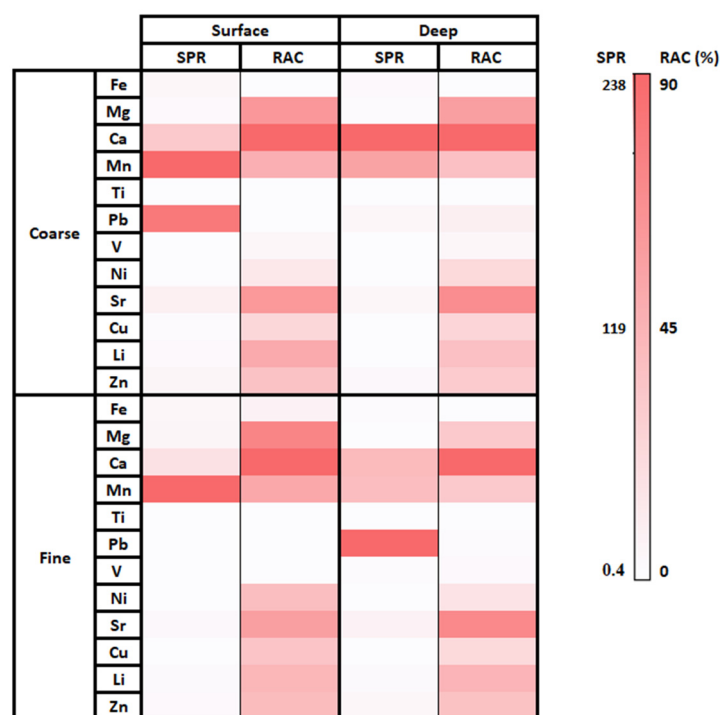
Figure 6. Secondary–primary phases ratio (SPR) and RAC values.

4. Discussion

The availability and quality of surface water are the current challenges to ensure its fair use. Suspended sediments are a comprehensive source of information to obtain the contribution of potentially toxic elements in aquatic ecosystems.

The physicochemical parameters regulate the chemical nature of metals that can participate in chemical reactions and be responsible for the accessibility of some of those chemical species to the biota. ORP showed lower values than those published [28,29], with values at a deeper level from 80 to 88 mV; suggesting a possible induction of reduction conditions at the bottom of this reservoir.

Suspended sediments are, according to grain size [54], in the interval of silts (0.004–0.063 mm) and clay (<0.004 mm). These suspended sediments are composed of calcite [Ca(CO$_3$)], quartz [(SiO$_2$)], albite [(Al$_{1.2}$Ca$_{0.2}$Na$_{0.8}$O$_8$Si$_{2.8}$)], and montmorillonite [Ca(Al$_2$Si$_4$O$_{11}$ (OH))]. Several authors have reported that clays (montmorillonite) are the main components of the suspended sediments in a river [14,55]. However, the composition of the sediment material in a reservoir can be attributed to the classification of the local rocks/soils, which under weathering process produce particles of different sizes, including some dissolved chemical species by leaching from these rocks. Previous studies of this reservoir found the same species in the sedimentary material at the bottom level [56]. Chemical partitioning help to understand the changes that metals suffer towards labile forms, allowing the metal availability for the environment. Some metals such as Cu, Ni, Pb, and Zn analyzed in these suspended sediments showed similar contents and distribution by partitioning to those published by other studies [6,52].

The adequate statistical treatment of the data to precisely describe the behavior of chemical species in environmental matrices is a challenge. The concentrations of elements in the geochemical assessment generally present a non-normal behavior. Thus, suspended sediments are a significant source of information about the contents and relationships of elements, which need to be adequately analyzed. According to PCA results, the elements are from natural origin, where depth and particle size do not influence metals' contents in the sediment matrix (Table 1, Figure S1 supplementary material). Nevertheless, particle size may be a relevant factor of scavenging under ion conditions of elements commonly present in dissolved fractions [1,8,12,19,55,57].

As shown in Figure 4, the concentrations of each element are not modified independently and freely, but were affected by the chemical behavior of the other elements and the environmental characteristics. Due to the elements being concentrated in suspended sediments, their composition was intimately related to the particle fractions. Furthermore, the elements are clustered within every fraction (Figure 4), indicating the co-occurrence of metals. Thus, Ca (>66%), Mg (>53%), Sr (>62), and Li (>32%) were dominantly found in the bioavailable fraction (F1). Moreover, metals such as Ca, Li, Mg, Fe, Cu, and Zn are grouped in this fraction (Figure 4a), where Li, Ca, and Mg are highly correlated (R > 0.92, *p* value < 0.05). According to the BCR scheme, those metals are linked to carbonates and are easily freed to the aquatic environment [58,59].

Major metals in the earth's crust tend to be linked to oxides released from the mineral matrix when conditions change from oxic to anoxic. The highest concentrations of Fe (>54%), Mn (>49%), Pb (>60%), and V (>44%) were in the reduced fraction (F2), most of them with a similar oxidation state (2+, 3+). In this fraction of particles, the elements were strongly correlated and distributed in three groups (Figure 4b): (a) Mn, Fe, and V (R > 0.95); (b) Sr, Ca, and Mg (R > 0.90); and (c) Li, Cu, Pb, and Zn (R > 0.90). According to cluster distributions, the two first groups are positively correlated and represent the major elements forming the mineral matrix of suspended sediments. The third group contains the trace elements and is distributed negatively to the first group (a) and weakly correlated to the second group (b); it probably indicates the adsorption of these trace elements onto the mineral matrix. The co-occurrence of Fe, Mn, and V in minerals is well known because of their similar geochemical process on earth's crust [57]. Likewise, it has been published that Pb concentrations are mainly found in the reduced fraction of bottom sediments [6,22,36]. In this fraction, some trace elements may be bounded to Fe-Mn oxides that would be released under reductive conditions, which suggests that Li, Cu, Pb, and Zn in suspended sediments are being released from Fe/Mn oxides/hydroxides, as in bottom sediments [21,22,60].

No metals were predominant in the oxidized fraction (F3); however, elements such as Li, Mg, Cu, Zn, and Sr are co-occurring in this fraction. Previous studies have demonstrated a high association (>40%) between Cu and organic components [6,52,61], but in this study, copper contents in the oxidized fraction are in a low range (from 14 to 18%). Finally, Ti was concentrated (49–80%) in the residual fraction (F4), indicating its conservative behavior as part of the mineral matrix. Two dominant groups were observed (R > 0.8); the first is formed by Sr, Zn, Ca, Li, and Cu, while the second is grouped by Mg, Mn, Ti, Fe, and Ni. These results coincide with those determined by the XRD and SEM-EDX analyses, where the presence of Ca- and Fe- minerals are observed.

Nevertheless, it is noticeable that considerable contents of Fe (12–40%) and V (36–45%) are also present in the residual fraction, while Mn contents (30–43%) are in the bioavailable fraction. This behavior has been reported previously, where the residual fraction of sediments and soil shown high iron concentrations [6,21,22,62] and, even a high percent of Mn has been detected in the reducible fraction of sediments from city streets [62], this metal is also bounded to carbonates in soil particles [21]. In addition, Zn also tended to be in exchangeable (26–36%) and reducible (24–42%) fractions, as has been reported in other studies, [52] and [6], respectively. Finally, Ti concentrations were also ranged from 20 to 40% in oxidized fraction. Therefore, a significant correlation between bioavailable-oxidized and reducible-residual fractions was observed (*p* value < 0.05) due to the similarity of metal co-occurrence in those sediment phases; it is shown in Figure 7.
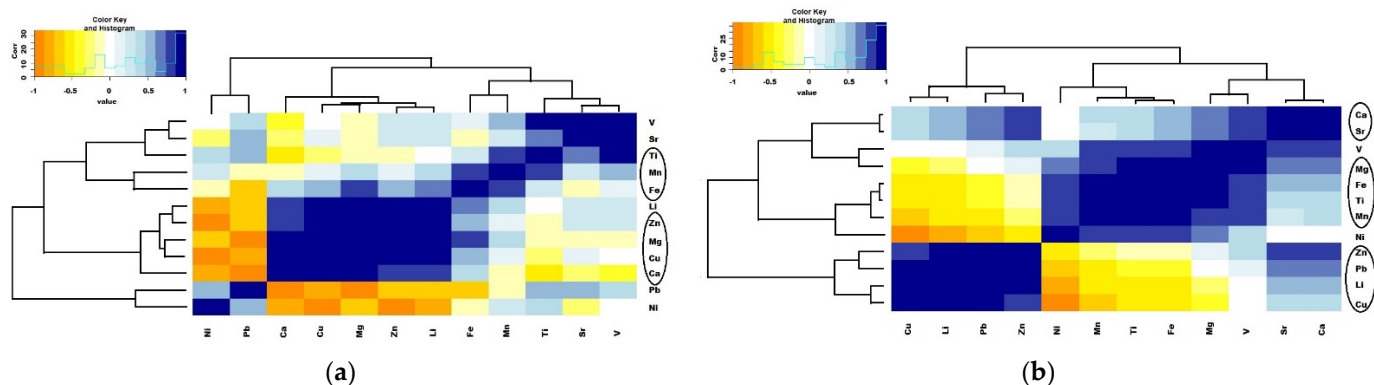
Figure 7. Co-occurrence of metals within integrated sediment fractions: (**a**) bioavailable-oxidized fraction and (**b**) reduced-residual fraction. Distinctive groups are highlighted by circles.

Here, the association and distribution of elements can be observed more clearly due to metal affinity. Thus, elements such as Ca, Cu, Mg, and Zn are grouped in the bioavailable-oxidized fraction (R > 0.85), which are elements classified as nutrients and tend to be present in organic material (Figure 7a). Likewise, the reduced-residual fraction shows three main clusters (R > 0.9; Figure 7b): (a) Ca-Sr, (b) Fe-Mn-Ti, and (c) trace elements. According to these groups, major elements are well defined in two groups, Ca-oxides/carbonates and Fe/Mn-oxyhydroxides, forming the mineral matrix of these sediments. Therefore, it may suggest that suspended sediments are particles produced by the physical and chemical erosion from both sedimentary rocks (limestone, dolomites, among others) and volcanic rocks (intermediate and basic composition) present in the study area [25,26].

On the other hand, lithology is a crucial parameter of high contents of isotopic uranium and thorium concentrations in water [15]. Thus, the radioisotopes ^{238}U, ^{234}U, ^{232}Th, and ^{230}Th were highly correlated (R > 0.8 and $p < 0.05$). In addition, isotopic uranium was found three-fold more concentrated in fine particles than in coarse particles ($p < 0.05$), whereas ^{230}Th and ^{232}Th did not show partitioning by size particle ($p < 0.05$).

The ^{234}U/^{238}U activity ratio is similar in both particles; this disequilibrium can be attributed mainly to the alpha recoil and the particle scavenging. Under oxidizing conditions, U is mainly in its mobile form (hexavalent) [15,37,63–67] and is maintained in solution due to the presence of CO_3^{2-} and HCO_3^{-} [68]. Conversely, Th is usually found in its immovable form (+IV) under these conditions. At a deep level of this reservoir, sub-oxic conditions tend to affect the uranium and thorium concentrations in coarse particles (R > 0.7). Moreover, alkalinity also controls the mobility of isotopic uranium in fine particles (R > −0.7). Likewise, isotopic U and Th increased their concentrations in these suspended sediments by increasing most metal contents, specifically Cu, Fe, Ti, and Zn. Moreover, ^{230}Th/^{232}Th activity ratio was above the unit, indicating thorium from the 238U disintegration chain (alpha recoil).

The radioactive decay of ^{238}U atom in a sediment particle produces alpha particles and daughter atoms, which can be ejected closer to the surface particle by the recoil energy. The alpha-recoil process promotes a radioactive daughter's mobilization from its initial position. Moreover, uranium might migrate to oxidation states (+6) during the alpha decay, obtaining a high solubility. In suspended sediments, >43% of isotopic uranium was found in the bioavailable fraction, which can be attributed to the alpha-recoil of uranium. Conversely, isotopic thorium was mainly found in the residual fraction of suspended sediments, ranging from 70% to 84% for ^{232}Th and from 49% to 70% for ^{230}Th, showing their natural origin.

The ^{234}U/^{238}U and ^{230}Th/^{238}U activity ratios were in secular equilibrium within the residual fraction of coarse particles. However, this was different in fine particles where ^{234}U/^{238}U and ^{230}Th/^{238}U were 4 and 8, respectively; it corroborates the metal scavenging by finer particles. Furthermore, the ^{232}Th/^{238}U activity ratio ranges from 2 to 8 in the

residual fraction, according to the abundance ratio in the earth's continental crust [47], corroborating the conservative behavior immobile condition for thorium.

Potential Pollution Risk

The degree of metals mobilization in aquatic ecosystems is controlled by their chemical and physical conditions and environmental parameters.

While Ca and Mg can be essential nutrients for living organisms, other metals as Pb and Cu are chemically persistent and can be accumulated by biota, transferring these elements to the food chain [69].

Mobile elements show similar or lesser concentrations in the solid phase than in the solution phase, showing kd values of tens [14], whereas kd values of 100 and 1000 correspond to intermediate and highly immobile elements, respectively. From the total concentrations of elements in suspended sediments, mobile metals were Mg, Ca, Sr, and U; intermediate mobile metals were Fe, V, Ni, Pb, Cu, Li, and Zn, while Ti, Mn, and Th were highly immobile (Table 1).

Due to their chemical affinity, Ca, Mg, and Sr are mainly associated in available phases, Figure 6b. The co-occurrence of those elements is also observed within the sediment matrix or forming oxisalts (Figure 6b), giving them a high mobility status. These mobile divalent metals were correlated with hardness and alkalinity at the surface level, R = 0.9 and R = 0.6, respectively. The water temperature in this level ranged from 16 to 20 °C, leading to the dissociation of Ca/Mg/Sr carbonates from suspended sediments, which, by releasing carbonates, increases the alkalinity of water. Furthermore, when Ca^- Mg^- CO_3 in water are in the presence of atmospheric CO_2 might give a temporary hardness. Meanwhile, on a deeper level, Ca and Mg were highly correlated with chlorides (R = 0.85), providing a total hardness.

On the other hand, although the element mobility can substantially describe the metal behavior in sediments, it is crucial to understand the co-occurrence of these chemical species within solid phases. For instance, Ti and Mn were detected as immobile elements (kd > 1000) and are commonly associated with the mineral matrix; however, considerable amounts of them were obtained in exchangeable phases of suspended sediments; Mn (F2) and Ti (F3). Iron is a chemical reducing agent co-occurring with those elements (Figure 7), leading them to form oxides/hydroxides; thus, Mn and Ti can modify their availability depending on the presence and interrelationship with other elements in solid phases. Therefore, these transition metals (Figure 7b) should be established as elements with intermediate mobility.

Most metals showed concentrations >60% within available fractions of suspended sediments. The metal release due to its availability generates a potential environmental risk [6,36,69,70]. Although metal concentrations in coarse and fine particles are higher than those reported in bottom sediments from surface water bodies and sea [14,60,69,71], these particles showed similarities of element partitioning in sediment fractions [6,7,9,22,36,49,57,58,72].

Due to particle morphology and fractionation of metals, most of them provided contamination factors ranging from moderate to very high levels; even these metals show heavy contamination levels by geoaccumulation, reaching severe enrichment (Figure 5); Zn, Li, Cu, Pb, and Mn contents in fine particles reached extremely severe enrichment. Previously, Pb was found to be moderately enriched in the bottom sediments of this reservoir [56] with a low coefficient of variation on its concentration. Thus, sediment resuspension from the bottom affects Pb contents in suspended sediments, which shows moderate-severe enrichment levels.

Similarly, Igeo values ranged from moderately to heavily contaminated, where the main contributors were Cu, Mn, Li, Pb, and Zn. Commonly, contamination by trace elements is associated with industrial activities and urban development [52,73–76]. However, in some sediments from areas with high population density and significant industrial activity, pollution by heavy metals was not detected [69].

The Ef and Igeo use gross information of the average element concentrations from the upper earth's crust and the metal normalization [11,45,49], but it does not consider

the intrinsic processes of water bodies and the chemical behavior of elements within solid phases. In an aqueous medium, some new solid phases might be formed when rocks suffer chemical weathering, particularly from carbonate and silicate rocks [77–79]. Due to that, these new/secondary solid phases tend to have low weight and small diameters. The finer particles show a high surface area with binding sites that easily trap toxic metals [19]. Morphologically, the coarse particles have well-defined shapes, showing rounded or sharp surfaces (Figure 2a–c); conversely, fine particles showed agglomerates formed by the attraction of charges from their surfaces (Figure 2d–f).

Consequently, some metals can be adsorbed/desorbed from sediments, accordingly their oxidation state. Due to this, these particles can promote the scavenging of these trace metals from the dissolved phase. Therefore, natural processes can also modify the metal concentrations in suspended sediments, turning them into a contamination source for water bodies [80,81].

Metal toxicity is often a function of metal concentration and availability [6,10,58]. In this reservoir, metals are concentrated in the available fractions of suspended sediments above the unit, where Ca, Mn, and Pb are highly concentrated in these secondary phases (SPR); the metals in those phases can only be released under specific conditions, oxidation-reduction conditions in the water. Nevertheless, the metals in bioavailable fraction (F1) are the most accessible metals for biota; some of those are essential nutrients for organisms. Finally, the metals such as Sr ($\geq$50%) > Mn=Li ($\geq$30%) > Cu=Ni ($\geq$20%) are being easily released, and consequently, might be the main contributor to the potential pollution risk for aquatic biota.

5. Conclusions

In this study, the partitioning, association, and geochemical fractionation of metals in suspended sediments were evaluated and used to establish the potential pollution risk of an aquatic ecosystem.

Suspended sediments showed a natural origin based on these results, produced by physical and chemical erosion from the surrounding rocks. However, some metals showed high concentrations linked to the exchangeable phases of suspended sediments.

The sediment phases were the main parameter affecting the partitioning and availability of metals, which are co-occurring due to their chemical affinity; nevertheless, the finer suspended sediments can act as scavengers of metals.

It was determined that metal concentration in sediments is highly dependent on the interrelation and co-occurrence of elements, inducing metals showing low solubility to modify their chemical conditions and migrate to phases that can be released into the surrounding environment. Although the distribution coefficient provides an overview of the mobility of elements, it is crucial to assess their availability within the solid phases. It will provide an accurate assessment of metal behavior and availability.

Pollution indices are a helpful tool for determining the potential pollution risk; however, these should be modified according to the availability of chemical species in the exchangeable phases of sediments. Thus, due to their concentrations and availability, metals such Sr, Mn, Li, Cu, and Ni are the main contributors to potential pollution risk for the aquatic environment under study.

Finally, the adequate statistical treatment of the geochemical data helps obtain a result closer to the occurrence and behavior of metals in the environmental evaluation. Likewise, chemical fractionation methodology improves the prediction of the potential pollution risk caused by metals(oids) in aquatic ecosystems.

Supplementary Materials: The following supporting information can be downloaded at: https://www.mdpi.com/article/10.3390/w14060980/s1, Table S1: Physiochemical parameters and chemical species in bulk water of the reservoir San Marcos; Table S2: Mean contents of major (% weight) and trace (mg kg^{-1}) elements and their range in suspended sediments and dissolved phase; Figure S1: Association of elements by particle size and depth: (a) surface coarse particles, (b) surface fine particles, (c) deep coarse particles, and (d) deep fine particles; Figure S2: The metal percent by particle

fractions: (a) Coarse particles at surface level, (b) Fine particles at the surface, (c) Coarse particles at deep level, and (d) Fine particles at a deep level. F1 (bioavailable fraction); F2 reduced fraction; F3 oxidized fraction; F4 residual fraction; Figure S3: Isotopic U and Th percent by fractions of coarse and fine particles at a deep level. F1 (bioavailable fraction); F2 reduced fraction; F3 oxidized fraction; F4 residual fraction.

References

1. Islam, M.S.; Ahmed, M.K.; Raknuzzaman, M.; Habibullah-Al-Mamun, M.; Islam, M.K. Heavy metal pollution in surface water and sediment: A preliminary assessment of an urban river in a developing country. *Ecol. Indic.* **2015**, *48*, 282–291. [CrossRef]
2. Toro, M.; Robles, S.; Avilés, J.; Nuño, C.; Vivas, S.; Bonada, N.; Prat, N.; Alba Tercedor, J.; Casas, J.; Guerrero, C.; et al. *Calidad de Las Aguas de Los Ríos Mediterráneos del Proyecto GUADALMED*; Características Físico-Químicas; Limnetica: Madrid, Spain, 2002; pp. 63–75.
3. Sophocleous, M. Interactions between groundwater and surface water: The state of the science. *Hydrogeol. J.* **2002**, *10*, 52–67. [CrossRef]
4. Lu, G.Y.; Wong, D.W. An adaptive inverse-distance weighting spatial interpolation technique. *Comput. Geosci.* **2008**, *34*, 1044–1055. [CrossRef]
5. Ruiz-Fernández, A.C.; Páez-Osuna, F.; Urrutia-Fucugauchi, J.; Preda, M. 210Pb geochronology of sediment accumulation rates in Mexico City Metropolitan Zone as recorded at Espejo de los Lirios lake sediments. *Catena* **2005**, *61*, 31–48. [CrossRef]
6. Ferrans, L.; Jani, Y.; Burlakovs, J.; Klavins, M.; Hogland, W. Chemical speciation of metals from marine sediments: Assessment of potential pollution risk while dredging, a case study in southern Sweden. *Chemosphere* **2021**, *263*, 128105. [CrossRef] [PubMed]
7. Williams, J.A.; Antoine, J. Evaluation of the elemental pollution status of Jamaican surface sediments using enrichment factor, geoaccumulation index, ecological risk and potential ecological risk index. *Mar. Pollut. Bull.* **2020**, *157*, 111288. [CrossRef] [PubMed]
8. Gloaguen, T.V.; Motta, P.N.S.D.; Couto, C.F. A grain-size correction for metal pollution indexes in river sediments. *Int. J. Sediment Res.* **2020**, *36*, 362–372. [CrossRef]
9. Saravanan, P.; Krishnakumar, S.; Silva, J.D.; Pradhap, D.; Vidyasakar, A.; Radhakrishnan, K.; Godson, P.S.; Arumugam, K.; Magesh, N.S. Elemental concentration and potential ecological risk assessment of reef associated surface sediments of Appa Island, Gulf of Mannar Biosphere Reserve, Southeast coast of India. *Mar. Pollut. Bull.* **2018**, *128*, 398–407. [CrossRef] [PubMed]
10. Tomlinson, D.L.; Wilson, J.G.; Harris, C.R.; Jeffrey, D.W. Problems in the assessment of heavy-metal levels in estuaries and the formation of a pollution index. *Helgoländer Meeresunters.* **1980**, *33*, 566–575. [CrossRef]
11. Hakanson, L. An ecological risk index for aquatic pollution control. A sedimentological approach. *Water Res.* **1980**, *14*, 975–1001. [CrossRef]
12. Rousseau, T.C.C.; Roddaz, M.; Moquet, J.-S.; Handt Delgado, H.; Calves, G.; Bayon, G. Controls on the geochemistry of suspended sediments from large tropical South American rivers (Amazon, Orinoco and Maroni). *Chem. Geol.* **2019**, *522*, 38–54. [CrossRef]
13. Oliveira, M.L.S.; Saikia, B.K.; da Boit, K.; Pinto, D.; Tutikian, B.F.; Silva, L.F.O. River dynamics and nanopaticles formation: A comprehensive study on the nanoparticle geochemistry of suspended sediments in the Magdalena River, Caribbean Industrial Area. *J. Clean. Prod.* **2019**, *213*, 819–824. [CrossRef]
14. Viers, J.; Dupré, B.; Gaillardet, J. Chemical composition of suspended sediments in World Rivers: New insights from a new database. *Sci. Total Environ.* **2009**, *407*, 853–868. [CrossRef] [PubMed]
15. Chabaux, F.; Bourdon, B.; Riotte, J. Chapter 3 U-Series Geochemistry in Weathering Profiles, River Waters and Lakes. In *Radioactivity in the Environment*; Porcelli, D., Krishnaswami, S., Cochran, J.K., Eds.; Elsevier: Amsterdam, The Netherlands, 2008; Volume 13, pp. 49–104.

16. Looi, L.J.; Aris, A.Z.; Yusoff, F.M.; Isa, N.M.; Haris, H. Application of enrichment factor, geoaccumulation index, and ecological risk index in assessing the elemental pollution status of surface sediments. *Environ. Geochem. Health* **2019**, *41*, 27–42. [CrossRef]

17. IAEA. *Handbook of Parameter Values for the Prediction of Radionuclide Transfer in Terrestrial and Freshwater Environments*; IAEA: Vienna, Austria, 2010; p. 200.

18. Ani, E.-C.; Wallis, S.; Kraslawski, A.; Agachi, P.S. Development, calibration and evaluation of two mathematical models for pollutant transport in a small river. *Environ. Model. Softw.* **2009**, *24*, 1139–1152. [CrossRef]

19. Batley, G.E.; Simpson, S. Sediment Quality Guidelines. In *Encyclopedia of Aquatic Ecotoxicology*; Férard, J.-F., Blaise, C., Eds.; Springer: Dordrecht, The Netherlands, 2013; pp. 1015–1024.

20. Warren, N.; Allan, I.J.; Carter, J.E.; House, W.A.; Parker, A. Pesticides and other micro-organic contaminants in freshwater sedimentary environments—A review. *Appl. Geochem.* **2003**, *18*, 159–194. [CrossRef]

21. Alan, M.; Kara, D. Comparison of a new sequential extraction method and the BCR sequential extraction method for mobility assessment of elements around boron mines in Turkey. *Talanta* **2019**, *194*, 189–198. [CrossRef] [PubMed]

22. Nemati, K.; Bakar, N.K.A.; Abas, M.R.; Sobhanzadeh, E. Speciation of heavy metals by modified BCR sequential extraction procedure in different depths of sediments from Sungai Buloh, Selangor, Malaysia. *J. Hazard. Mater.* **2011**, *192*, 402–410. [CrossRef] [PubMed]

23. Pérez-López, R.; Álvarez-Valero, A.M.; Nieto, J.M. Changes in mobility of toxic elements during the production of phosphoric acid in the fertilizer industry of Huelva (SW Spain) and environmental impact of phosphogypsum wastes. *J. Hazard. Mater.* **2007**, *148*, 745–750. [CrossRef] [PubMed]

24. Tessier, A.; Campbell, P.G.C.; Bisson, M. Sequential extraction procedure for the speciation of particulate trace metals. *Anal. Chem.* **1979**, *51*, 844–851. [CrossRef]

25. Reyes-Cortés, M.; Reyes-Cortés, I.A.; Espino Valdez, S.; Rentería-Villalobos, M.; Burillo Montúfar, J.C.; Montero-Cabrera, M.E. Origen y distribución de la radiactividad natural en la zona norte de la cuenca de Chihuahua, México. *Rev. Mex. Cienc. Geológicas* **2012**, *29*, 659–675.

26. Ferríz, H. Uranium mineralization in the San Marcos volcanic center Chihuahua, Mex. In Proceedings of the Uranium Deposits in Volcanic Rocks, El Paso, TX, USA, 2–5 April 1984; pp. 197–216.

27. INEGI. *Compendio de Información Geográfica Municipal*; INEGI: Aguascalientes City, Mexico, 2017.

28. Rentería-Villalobos, M.; Cortés, M.R.; Mantero, J.; Manjón, G.; García-Tenorio, R.; Herrera, E.; Montero-Cabrera, M.E. Uranium in the Surrounding of San Marcos-Sacramento River Environment (Chihuahua, Mexico). *Sci. World J.* **2012**, *2012*, 13. [CrossRef] [PubMed]

29. Burillo Montufar, J.C.; Reyes Cortés, M.; Reyes Cortés, I.A.; Espino Valdez, M.S.; Hinojosa de la Garza, O.R.; Nevárez Ronquillo, D.P.; Herrera Peraza, E.; Rentería Villalobos, M.; Montero Cabrera, M.E. Uranium-series isotopes transport in surface, vadose and ground waters at San Marcos uranium bearing basin, Chihuahua, Mexico. *Appl. Geochem.* **2012**, *27*, 1111–1122. [CrossRef]

30. NOM-014-SSA1-1993. Sanitary Procedures for the sampling of water for human use and consumption in public and private water supply systems. (Procedimientos Sanitarios para el muestreo de agua para uso y consumo humano en sistemas de abastecimiento de agua públicos y privados). Official Mexican Standard. Enviromental Health. Mexico, H.a.A.D., Ed.; DOF, Diario Oficial de la Federación, Secretaria de Economía: Mexico City, Mexico, 1993.

31. NMX-AA-072-SCFI-2001. In *Water Analysis—Determination of Total Hardness in Natural, Wastewaters and Wastewaters Treated—Test Method*; DOF, Diario Oficial de la Federación, Secretaría de Economía: Mexico City, Mexico, 2001; pp. 1–14.

32. NMX-AA-073-SCFI-2001. In *Water Analysis—Determination of Total Chlorine in Natural Water, Wastewaters and Wastewaters Treated—Test Method*; DOF, Diario Oficial de la Federación, Secretaria de Economía: Mexico City, Mexico, 2001; pp. 1–13.

33. NMX-AA-036-SCFI-2001. In *Water Analysis—Determination of Acidity and Total Alkalinity in Natural, Drinking, Wastewaters and Treated Wastewaters*; Secretaría de Comercio y Fomento Industrial, Secretaria de Economía: Mexico City, Mexico, 2001; pp. 1–22.

34. Hach Company. *Procedures Manual, DR/2010 Spectrophotometer: Photometric, Titration, and Microbiological Procedures*, 3rd ed.; Hach Company: Loveland, CO, USA, 2000; p. 874.

35. NMX-AA-051-SCFI-2001. In *Water Analisis—Determination of Metals By Atomic Absorption in Natural, Drinking, Wastewaters and Wastewaters Treated—Test Method*; DOF, Diario Oficial de la Federación, Secretaria de Economía: Mexico City, Mexico, 2001; pp. 1–47.

36. Mondal, P.; Schintu, M.; Marras, B.; Bettoschi, A.; Marrucci, A.; Sarkar, S.K.; Chowdhury, R.; Jonathan, M.P.; Biswas, J.K. Geochemical fractionation and risk assessment of trace elements in sediments from tide-dominated Hooghly (Ganges) River Estuary, India. *Chem. Geol.* **2020**, *532*, 119373. [CrossRef]

37. Pérez-Moreno, S.M.; Gázquez, M.J.; Pérez-López, R.; Bolivar, J.P. Validation of the BCR sequential extraction procedure for natural radionuclides. *Chemosphere* **2018**, *198*, 397–408. [CrossRef]

38. Degueldre, C.; Kline, A. Study of thorium association and surface precipitation on colloids. *Earth Planet. Sci. Lett.* **2007**, *264*, 104–113. [CrossRef]

39. Chabaux, F.; Riotte, J.; Dequincey, O. U-Th-Ra Fractionation during Weathering and River Transport. In *Uranium Series Geochemistry: Reviews in Mineralogy and Geochemistry*; Bourdon, B., Henderson, G.M., Lundstrom, C.C., Turner, S.P., Eds.; Mineralogical Society of America: Chantilly, VA, USA, 2003; pp. 1–19.

40. Kynčlová, P.; Hron, K.; Filzmoser, P. Correlation Between Compositional Parts Based on Symmetric Balances. *Math. Geosci.* **2017**, *49*, 777–796. [CrossRef]

41. SAS. *Statistical Analysis System Users' Guide*; Statistical Analysis System Institute, Inc.: Cary, NC, USA, 2006.

42. Boente, C.; Martín-Méndez, I.; Bel-Lán, A.; Gallego, J.R. A novel and synergistic geostatistical approach to identify sources and cores of Potentially Toxic Elements in soils: An application in the region of Cantabria (Northern Spain). *J. Geochem. Explor.* **2020**, *208*, 106397. [CrossRef]

43. Tarvainen, T.; Sapon, S.; Jarva, J. Applying heatmaps in interpretation of geochemical baseline data on urban soils in Finland. *J. Geochem. Explor.* **2019**, *205*, 106345. [CrossRef]

44. Reimann, C.; Filzmoser, P.; Garrett, R.G. Factor analysis applied to regional geochemical data: Problems and possibilities. *Appl. Geochem.* **2002**, *17*, 185–206. [CrossRef]

45. Barbieri, M. The Importance of Enrichment Factor (EF) and Geoaccumulation Index (Igeo) to Evaluate the Soil Contamination. *J. Geol. Geophys.* **2016**, *5*, 237. [CrossRef]

46. Sutherland, R.A.; Tolosa, C.A.; Tack, F.M.G.; Verloo, M.G. Characterization of Selected Element Concentrations and Enrichment Ratiosin Background and Anthropogenically Impacted Roadside Areas. *Arch. Environ. Contam. Toxicol.* **2000**, *38*, 428–438. [CrossRef] [PubMed]

47. Rudnick, R.L. Earth's Continental Crust. In *Encyclopedia of Geochemistry: A Comprehensive Reference Source on the Chemistry of the Earth*; White, W.M., Ed.; Springer International Publishing: Cham, Switzerland, 2018; pp. 392–418.

48. Rudnick, R.L.; Gao, S. Composition of the Continental Crust. *Treatise Geochem.* **2003**, *3*, 659. [CrossRef]

49. Birch, G.F. An assessment of aluminum and iron in normalisation and enrichment procedures for environmental assessment of marine sediment. *Sci. Total Environ.* **2020**, *727*, 138123. [CrossRef]

50. Lin, Q.; Peng, X.; Liu, B.; Min, F.; Zhang, Y.; Zhou, Q.; Ma, J.; Wu, Z. Aluminum distribution heterogeneity and relationship with nitrogen, phosphorus and humic acid content in the eutrophic lake sediment. *Environ. Pollut.* **2019**, *253*, 516–524. [CrossRef]

51. Mora, A.; Jumbo-Flores, D.; González-Merizalde, M.; Bermeo-Flores, S.A. Niveles de Metales Pesados En Sedimentos de La Cuenca Del Río Puyango, Ecuador. *Rev. Int. Contam. Ambient.* **2016**, *32*, 13. [CrossRef]

52. Xia, F.; Zhang, C.; Qu, L.; Song, Q.; Ji, X.; Mei, K.; Dahlgren, R.A.; Zhang, M. A comprehensive analysis and source apportionment of metals in riverine sediments of a rural-urban watershed. *J. Hazard. Mater.* **2020**, *381*, 121230. [CrossRef] [PubMed]

53. Reimann, C.; Filzmoser, P.; Hron, K.; Kynčlová, P.; Garrett, R.G. A new method for correlation analysis of compositional (environmental) data—A worked example. *Sci. Total Environ.* **2017**, *607–608*, 965–971. [CrossRef] [PubMed]

54. Franz, G.; Leitão, P.; Pinto, L.; Jauch, E.; Fernandes, L.; Neves, R. Development and validation of a morphological model for multiple sediment classes. *Int. J. Sediment Res.* **2017**, *32*, 585–596. [CrossRef]

55. Tian, S.; Li, Z.; Wang, Z.; Jiang, E.; Wang, W.; Sun, M. Mineral composition and particle size distribution of river sediment and loess in the middle and lower Yellow River. *Int. J. Sediment Res.* **2020**, *36*, 392–400. [CrossRef]

56. Méndez-García, C.G. *Reconstrucción Histórica de la Contaminación Por Arsénico, Plomo y Uranio en Los Sedimentos de Las Represas San Marcos y Luis L. León, en Chihuahua*; Original Research; Centro de Investigación en Materiales Avanzados, CIMAV: Chihuahua, Mexico, 2014; p. 148.

57. Telfeyan, K.; Breaux, A.; Kim, J.; Cable, J.E.; Kolker, A.S.; Grimm, D.A.; Johannesson, K.H. Arsenic, vanadium, iron, and manganese biogeochemistry in a deltaic wetland, southern Louisiana, USA. *Mar. Chem.* **2017**, *192*, 32–48. [CrossRef]

58. Soliman, N.F.; El Zokm, G.M.; Okbah, M.A. Risk assessment and chemical fractionation of selected elements in surface sediments from Lake Qarun, Egypt using modified BCR technique. *Chemosphere* **2018**, *191*, 262–271. [CrossRef]

59. Fernández-Ondoño, E.; Bacchetta, G.; Lallena, A.M.; Navarro, F.B.; Ortiz, I.; Jiménez, M.N. Use of BCR sequential extraction procedures for soils and plant metal transfer predictions in contaminated mine tailings in Sardinia. *J. Geochem. Explor.* **2017**, *172*, 133–141. [CrossRef]

60. Yuan, C.G.; Shi, J.B.; He, B.; Liu, J.F.; Liang, L.N.; Jiang, G.B. Speciation of heavy metals in marine sediments from the East China Sea by ICP-MS with sequential extraction. *Environ. Int.* **2004**, *30*, 769–783. [CrossRef] [PubMed]

61. Bruder-Hubscher, V.; Lagarde, F.; Leroy, M.J.F.; Coughanowr, C.; Enguehard, F. Application of a sequential extraction procedure to study the release of elements from municipal solid waste incineration bottom ash. *Anal. Chim. Acta* **2002**, *451*, 285–295. [CrossRef]

62. Kartal, Ş.; Aydın, Z.; Tokalıoğlu, Ş. Fractionation of metals in street sediment samples by using the BCR sequential extraction procedure and multivariate statistical elucidation of the data. *J. Hazard. Mater.* **2006**, *132*, 80–89. [CrossRef]

63. Riedel, T.; Kübeck, C. Uranium in groundwater–a synopsis based on a large hydrogeochemical data set. *Water Res.* **2018**, *129*, 29–38. [CrossRef] [PubMed]

64. Priestley, S.C.; Payne, T.E.; Harrison, J.J.; Post, V.E.A.; Shand, P.; Love, A.J.; Wohling, D.L. Use of U-isotopes in exploring groundwater flow and inter-aquifer leakage in the south-western margin of the Great Artesian Basin and Arckaringa Basin, central Australia. *Appl. Geochem.* **2018**, *98*, 331–344. [CrossRef]

65. Noli, F.; Kazakis, N.; Vargemezis, G.; Ioannidou, A. The uranium isotopes in the characterization of groundwater in the Thermi-Vasilika region, northern Greece. *Isot. Env. Health Stud.* **2016**, *52*, 405–413. [CrossRef] [PubMed]

66. Yamamoto, M.; Tomita, J.; Sakaguchi, A.; Ohtsuka, Y.; Hoshi, M.; Apsalikov, K. Uranium isotopes in well water samples as drinking sources in some settlements around the Semipalatinsk Nuclear Test Site, Kazakhstan. *J. Radioanal. Nucl. Chem.* **2010**, *284*, 309–314. [CrossRef]

67. Reyes, E.; Marques, L.S. Uranium series disequilibria in ground waters from a fractured bedrock aquifer (Morungaba Granitoids–Southern Brazil): Implications to the hydrochemical behavior of dissolved U and Ra. *Appl. Radiat. Isot.* **2008**, *66*, 1531–1542. [CrossRef] [PubMed]

68. Osmond, J.K.; Ivanovich, M. Uranium-series mobilization and surface hydrology. In *Uranium-Series Disequilibrium: Applications to Earth, Marine, and Environmental Science*; Ivanovich, M., Harmon, R.S., Eds.; Clarendon Press: Oxford, UK, 1992; pp. 259–289.

69. Fan, J.; Jian, X.; Shang, F.; Zhang, W.; Zhang, S.; Fu, H. Underestimated heavy metal pollution of the Minjiang River, SE China: Evidence from spatial and seasonal monitoring of suspended-load sediments. *Sci. Total Environ.* **2020**, *760*, 142586. [CrossRef] [PubMed]

70. Yu, Z.; Liu, E.; Lin, Q.; Zhang, E.; Yang, F.; Wei, C.; Shen, J. Comprehensive assessment of heavy metal pollution and ecological risk in lake sediment by combining total concentration and chemical partitioning. *Environ. Pollut.* **2021**, *269*, 116212. [CrossRef] [PubMed]

71. Burton, J.G.A. Sediment quality criteria in use around the world. *Limnology* **2002**, *3*, 65–76. [CrossRef]

72. Jorfi, S.; Maleki, R.; Jaafarzadeh, N.; Ahmadi, M. Pollution load index for heavy metals in Mian-Ab plain soil, Khuzestan, Iran. *Data Brief* **2017**, *15*, 584–590. [CrossRef]

73. Guan, Q.; Cai, A.; Wang, F.; Wang, L.; Wu, T.; Pan, B.; Song, N.; Li, F.; Lu, M. Heavy metals in the riverbed surface sediment of the Yellow River, China. *Environ. Sci. Pollut. Res.* **2016**, *23*, 24768–24780. [CrossRef]

74. Aiman, U.; Mahmood, A.; Waheed, S.; Malik, R.N. Enrichment, geo-accumulation and risk surveillance of toxic metals for different environmental compartments from Mehmood Booti dumping site, Lahore city, Pakistan. *Chemosphere* **2016**, *144*, 2229–2237. [CrossRef] [PubMed]

75. Zahra, A.; Hashmi, M.Z.; Malik, R.N.; Ahmed, Z. Enrichment and geo-accumulation of heavy metals and risk assessment of sediments of the Kurang Nallah—Feeding tributary of the Rawal Lake Reservoir, Pakistan. *Sci. Total Environ.* **2014**, *470–471*, 925–933. [CrossRef] [PubMed]

76. Varol, M. Assessment of heavy metal contamination in sediments of the Tigris River (Turkey) using pollution indices and multivariate statistical techniques. *J. Hazard. Mater.* **2011**, *195*, 355–364. [CrossRef]

77. Gaillardet, J.; Viers, J.; Dupré, B. 7.7—Trace Elements in River Waters. In *Treatise on Geochemistry*, 2nd ed.; Holland, H.D., Turekian, K.K., Eds.; Elsevier: Oxford, UK, 2014; pp. 195–235.

78. Gaillardet, J.; Dupré, B.; Allègre, C.J. Geochemistry of large river suspended sediments: Silicate weathering or recycling tracer? *Geochim. Cosmochim. Acta* **1999**, *63*, 4037–4051. [CrossRef]

79. Sun, H.; Han, J.; Li, D.; Zhang, S.; Lu, X. Chemical weathering inferred from riverine water chemistry in the lower Xijiang basin, South China. *Sci. Total Environ.* **2010**, *408*, 4749–4760. [CrossRef] [PubMed]

80. Zhang, Y.; Li, H.; Yin, J.; Zhu, L. Risk assessment for sediment associated heavy metals using sediment quality guidelines modified by sediment properties. *Environ. Pollut.* **2021**, *275*, 115844. [CrossRef] [PubMed]

81. Almeida, L.C.; da Silva Júnior, J.B.; dos Santos, I.F.; de Carvalho, V.S.; de Santana Santos, A.; Hadlich, G.M.; Ferreira, S.L.C. Assessment of toxicity of metals in river sediments for human supply: Distribution, evaluation of pollution and sources identification. *Mar. Pollut. Bull.* **2020**, *158*, 111423. [CrossRef] [PubMed]